Snowmelt runoff modelling in an arid mountain watershed, Tarim Basin, China

Xingong Li[1]* and Mark W. Williams[2]

[1] *Department of Geography, University of Kansas, Lawrence, KS 66045 USA*
[2] *Institute of Arctic and Alpine Research and Department of Geography, University of Colorado, Boulder, CO 80309 USA*

Abstract:

The feasibility of simulating daily snowmelt runoff in an arid mountain watershed with limited hydro-meteorological measurements was explored with an enhanced temperature-index snowmelt runoff model (SRM) in which the degree-day factor (DDF) is varied on the basis of shortwave solar radiation and snow albedo. The model satisfactorily simulated snowmelt runoff with a model efficiency of 0·64 for the calibration year and efficiency values of 0·78 and 0·51 for two validation years. Analysis indicated that the model was sensitive to lapse rate and snow albedo parameterization. The distinct seasonal variation of lapse rate played a key role for successful simulation. Snow albedo parameterization, which directly scaled snow cover percentage into snow albedo, worked quite well for the watershed although further validation is needed. Eight-day snow cover data from the Moderate Resolution Imaging Spectroradiometer (MODIS) were used to feed the model. A frequency filter, which filtered out the clouds and large fluctuation of snow cover from the MODIS snow cover data, also improved model performance. The model, however, did not simulate peak stream flows well as most of the model runs underestimated them. Copyright © 2008 John Wiley & Sons, Ltd.

KEY WORDS   temperature-index modelling; solar radiation; snow albedo

Received 2 December 2007; Accepted 22 May 2008

INTRODUCTION

Arid lands are home to some 15% of the world's population (Findlay, 1998). For many of the arid lands, mountain-fed rivers are the only available water resources to cover the needs for public supply, agriculture irrigation, hydropower and other uses. Snow and glaciers in those mountain basins play an important role in forming the flow regime which depends on snow and glacier melt rather than the timing of precipitation. Much of the value of this meltwater as a resource lies in its reliable occurrence at a particular time of the year, and is enhanced if total melt-season runoff and its day-to-day timing can be predicted. Accurate forecasting can also minimize the risk and loss from floods caused by rapid snow and glacier melt (Ferguson, 1999). In addition, potential impacts of climate change (IPCC, 2007) on stream-flow regimes could be evaluated if valid snow-/glacier-melt runoff models are available.

Located at the centre of Eurasia in western China, the Yarkant River is an arid mountain river which originates from the lofty Karakorum Mountains, traverses the oases scattered along its waterway in the Taklimakan Desert, and finally flows into the Tarim River, the longest continental river in the world. The mountain basin covers an area of about 50 000 km² with an average elevation of 4500 m and the runoff is generated primarily through snow and glacier melting. The river runs across a fluvial and desert plain where it provides water for 1·7 million people and for the largest irrigated agriculture lands in the region. With an extremely low annual precipitation of about 50 mm, water supply in the plain depends primarily on snow-/glacier-melt runoff from the mountain basin. The location, climate, and elevation of the mountain basin make it a unique watershed to study.

Both energy-balance models and temperature-index approaches have been developed and used to model snow and ice melt in many mountain watersheds. Although energy balance models have a solid physical basis, they are often not practical because of the large data requirements, especially in data-scarce mountain watersheds. Temperature-index models, on the other hand, are commonly used because of generally good performance, low data requirements, and computational simplicity. The degree-day factor (DDF) in temperature-index models is a key parameter, which summarizes the complex interaction among various energy components. Seasonal variation of DDF has long been noticed and various efforts have been made to either vary DDF as a function of other variables (Braun *et al*., 1993; Schreider *et al*., 1997; Arendt and Sharp, 1999; Daly *et al*., 2000) or to formulize models where shortwave radiation and/or snow albedo are included (Cazorzi and Dalla Fontana, 1996; Kane and Gieck, 1997; Dunn and Colohan, 1999; Hock, 1999; Pellicciotti *et al*., 2005).

An important issue in applying snowmelt runoff models is the physical accessibility and the lack of hydro-meteorological measurements in high-altitude mountain

* Correspondence to: Xingong Li, Department of Geography, University of Kansas, Lawrence, KS 66213. E-mail: lixi@ku.edu

watersheds. The objective of this research is to explore the feasibility of modelling snowmelt runoff in a data-sparse mountain watershed in the Yarkant River basin. In this study, we modified existing snowmelt models to develop methods appropriate for such a data-scarce mountainous area and identify primary data limitations. We developed an enhanced temperature-index model which uses satellite-derived snow cover data and varies DDF based on shortwave solar radiation and snow albedo.

STUDY WATERSHED AND DATA

The Tizinapu basin, a tributary watershed of the Yarkant River, was selected for this study as the first attempt of modelling the entire Yarkant mountain watershed (Figure 1(a)). The Tizinapu sub-watershed is located in the northeast part of the Yarkant mountain watershed. It covers an area of 5518 km^2 with a mean elevation of 3605 m. The primary land covers in the watershed are bare ground (51%), open shrubland (35%), grassland (9%), and wood/grassland (5%). Meltwater in the watershed is primarily from snow, although there are glaciers in the watershed. For simplicity, snow and glacier were not distinguished in this study.

Daily stream flow, precipitation, and temperature measurements were collected at the Yuzimen hydro-meteorological station, which is located at the outlet of the watershed (Figure 1(a)). Average annual precipitation at the station is 120 mm and average minimum and maximum temperatures are $-12\,°C$ and $29\,°C$, respectively. The digital elevation model (DEM) from the space-shuttle radar topography mapping (SRTM) mission, which has a spatial resolution of 90 m, was used in the study. The holes in the SRTM DEM were filled with USGS GTOPO30 DEM which has a spatial resolution of 1 km. Elevation in the watershed ranges between 1575 and 6234 m (Figure 1(b)). Snow-cover products, derived from the Moderate Resolution Imaging Spectroradiometer (MODIS) were used to provide snow cover area and

to estimate snow albedo (Hall *et al.*, 2002). The products provide global daily and 8-day maximum snow cover extent at 500-m spatial resolution.

THE MODEL

Snowmelt estimate

Many studies have shown considerable improvements on snowmelt runoff modelling by incorporating short-wave solar radiation in the modified temperature-index models (Cazorzi and Dalla Fontana, 1996; Kane and Gieck, 1997; Hock, 1999; Pellicciotti *et al.*, 2005). Particularly, Pipes and Quick (1987) found that solar radiation-based temperature-index models gave far better results in a heavily glacierized Karakoram basin where conventional temperature-index models drastically underestimated radiation melt at higher elevation. Research from U.S. Army Corps of Engineers (USACE) also concluded that although temperature is a reasonable good index of energy flux in heavily forested areas, it is less so in open areas where shortwave radiation or wind velocity plays a more important role in the melt process (USACE, 1998).

Snow albedo determines the amount of incoming solar radiation that is absorbed at snow surface and is therefore a significant control on surface snowmelt (Bloschl, 1991; Brock *et al.*, 2000). The dependence of DDF on albedo has been established in several researches (Schreider *et al.*, 1997; Arendt and Sharp, 1999). Pellicciotti *et al.* (2005) also attributed the better performance of their enhanced temperature-index model to the inclusion of albedo in their shortwave radiation term. They concluded that the inclusion of albedo eliminated the need to adjust the melt factor over the ablation season.

Based on the Snowmelt Runoff Model (SRM) (Martinec, 1975; Martinec and Rango, 1986) and previous researches (especially Cazorzi and Dalla Fontana, 1996; Hock, 1999; Pellicciotti *et al.*, 2005), an enhanced temperature-index model that incorporates shortwave solar radiation and snow albedo was developed. The
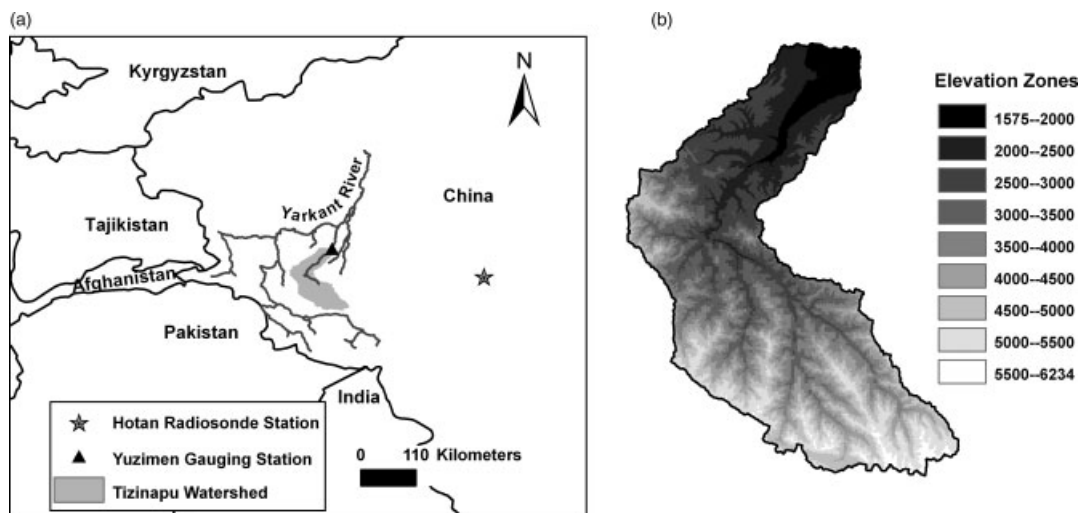

Figure 1. Geographic location of the Tizinapu mountain watershed (a) and the nine elevation zones used in the model (b)

model is not intended to create a semi-physically based model where temperature-independent energy components are added to a conventional temperature-index model. Such an effort is hindered by the lack of accessibility and measurements in the studied mountain watershed. Instead, our model can be thought of as a conventional temperature-index model where the DDF is varied by solar radiation and snow albedo. The model calculates daily snowmelt at a point with the following equation:

$$M = \begin{cases} m \times R \times (1 - \alpha) \times (T_d - T_0) & T_d > T_0 \\ 0 & T_d <= T_0 \end{cases} \tag{1}$$

where M (cm day^{-1}) is daily snowmelt, T_d (°C) is daily mean temperature, T_0 (°C) is a threshold temperature beyond which melt occurs, α is surface albedo without unit, R (W h m^2 day^{-1}) is the daily total shortwave solar radiation (direct plus diffuse), and m (m^2 cm W^{-1} h^{-1} °C^{-1}) is a composite parameter which is the multiplication of the melt factor and the snow runoff coefficient in SRM and a radiation coefficient. Owing to the lack of observations, T_0 was assumed to be 0 °C for the study watershed.

With the wide range of elevation, the watershed was divided into nine elevation zones, with each zone having an elevation range of about 500 m (Figure 1(b)). Those elevation zones are the spatial units of the model. Daily discharge from an elevation zone is calculated as:

$$V_i = (M_i \times S_i + c \times P_i) \times A_i \times \frac{10\,000}{86\,400} \tag{2}$$

where V_i (m^3 s^{-1}) is the average daily discharge from the ith zone, M_i (cm day^{-1}) is daily snowmelt in the ith zone calculated by Equation (1), S_i is snow cover percentage in the ith zone without a unit, c is precipitation runoff coefficient without a unit, P_i (cm day^{-1}) is daily precipitation in the ith zone, A_i is the size of the ith zone in km^2, and the constant 10 000/86 400 converts cm km^2 day^{-1} to m^3 s^{-1}.

Similar to SRM, a critical temperature (T_c), which is set to 0 °C for the study watershed for simplicity, is also used in our model to decide whether a precipitation event will be treated as rain or snow. In SRM, new snow from a precipitation event is kept in storage and then melted as soon as a sufficient number of degree-days have occurred. Different from SRM, our model does not keep track of new snow, as the precipitation extrapolated from the Yuzimen station is less reliable than the snow cover data derived from remote sensing observations.

Solar radiation

Many solar radiation models based on DEM have been developed (Dozier and Frew, 1990; Fu and Rich, 1999; Thornton *et al.*, 2000). These models differ in their methods of calculating atmospheric transmittance, direct and diffuse partitioning, and topographic modification. The solar-radiation model developed by Fu and Rich (1999) was used in this study because it is readily available in a geographic information system (GIS) environment

and accounts for typical atmospheric conditions, elevation, surface orientation, and influences of surrounding topography.

The model calculates the total solar radiation as the sum of direct and diffuse radiation while neglecting reflected radiation. The calculation involves the generation of an upward-looking hemispherical viewshed based on topography, the overlay of the viewshed on a direct sunmap to estimate direct radiation, and the overlay of the viewshed on a diffuse skymap to estimate diffuse radiation (more details can be found in Fu and Rich, 1999). The diffusion proportion parameter, which decides the proportion of global normal radiation flux that is diffused, was set to 0·3 indicating generally clear sky conditions. The transmittivity of the atmosphere, which controls the fraction of solar flux outside the atmosphere that passes through the atmosphere, was set to 0·5 indicating a generally clear sky. Daily total solar radiation at each cell in the watershed was first calculated and average daily total solar radiation in the nine elevation zones was then derived. This model thus assumes generally clear-sky conditions and does not account for differences in solar radiation caused by cloud cover.

Snow albedo

Computationally simple models, which estimate snow albedo as a function of snow age using simple decay functions (USACE, 1956; Kondo and Yamazaki, 1990) or as a logarithmic function of accumulated daily maximum positive temperature since snowfall (Brock *et al.*, 2000; Pellicciotti *et al.*, 2005), have been widely used in hydrology. In this study, two snow albedo parameterizations were used and compared. The first parameterization used Kondo and Yamazaki's (1990) model which requires only one parameter. The model assumes that albedo decreases exponentially with time (days) since the last snowfall as

$$\alpha_n = \alpha_{\min} + (\alpha_{\max} - \alpha_{\min})e^{-\frac{n}{k}} \tag{3}$$

where α_n is the albedo for nth day from the last snowfall, $\alpha_{\min}$ is minimum albedo, $\alpha_{\min}$ is maximum albedo, and k is a parameter representing the rate of decrease. Since snowfall events at higher elevations may not be reliably extrapolated from the only weather station at the lowest elevation of the watershed, snowfalls were identified from MODIS snow cover data.

The second albedo parameterization directly scales MODIS daily snow cover percentage into snow albedo using the following equation:

$$\alpha_n = \alpha_{\min} + \frac{(\alpha_{\max} - \alpha_{\min})}{S_{\max} - S_{\min}}(S_n - S_{\min}) \tag{4}$$

where α_n, $\alpha_{\min}$, and $\alpha_{\max}$ are the same as in Equation (3), S_n is the nth day snow cover percentage, $S_{\min}$ and $S_{\max}$ are the minimum and maximum snow cover percentages in a year, respectively. According to Equation (4), when the watershed has its maximum snow coverage (usually in late spring), its snow albedo is also the highest, and when

the watershed has its minimum snow coverage (usually in late summer), snow albedo is at its lowest point providing more energy from solar radiation for snowmelt. In both parameterizations, α_{min} and α_{min} were set to 0·4 and 0·9, respectively, based on Kondo and Yamazaki (1990).

Runoff routing

Detailed physics-based models have been developed and could in principle be used to route meltwater. However, most snowmelt runoff models simplify the processes using a small number of stores connected in series and still give good daily predictions (Ferguson, 1999). Our model used the same method in SRM to route both snowmelt and rain water to the watershed outlet. The method uses a single non-linear store, which is controlled by a recession coefficient k, as

$$Q_{n+1} = V_n(1 - k_{n+1}) + Q_n k_{n+1} \qquad (5)$$

where V is the sum of the total water (snowmelt plus rain water) from all the zones, Q is the average daily discharge at the watershed outlet, k is the recession coefficient, and n is the sequence of days in the simulation. Equation (5) is specific for a time lag of about 18 h between the daily temperature cycle and the resulting discharge cycle. For such a time lag, the computed total water on the nth day is assumed to contribute to the discharge on the $(n + 1)$th day and days after that. This time lag and therefore Equation (5) was estimated for the study watershed from its hydrographs and was verified by the empirical relationship between watershed size and lag time found in Martinec and Rango (1986). The recession coefficient k indicates the decline of discharge in a period without snowmelt and rainfall, and is assumed to vary inversely with discharge as

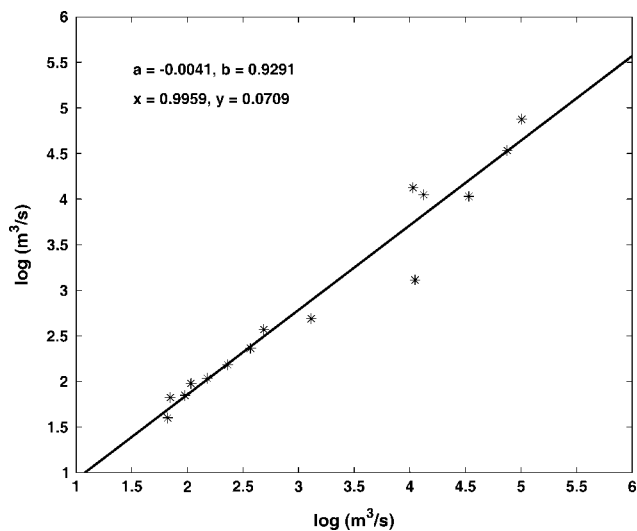$$k_{n+1} = \frac{Q_{n+1}}{Q_n} = xQ_n{}^y \qquad (6)$$

Figure 2. Scatter plot and linear regression of logarithmic recession discharges of year 2004 used to calculate parameters x and y in Equation (6)

Equation (6) can be reformatted by taking the natural log on both sides of the equation:

$$\ln(Q_{n+1}) = \ln(xQ_n{}^{(1-y)}) = \ln(x) + (1 - y)\ln(Q_n)$$
$$= a + b\ln(Q_n) \qquad (7)$$

where $a = \ln(x)$ and $b = 1 - y$. Parameters a and b in Equation (7), and then parameters x and y in Equation (6), can be obtained through linear regression with observed recession discharge data. Using the recession discharge data in 2004, parameters x and y were calculated as 0·9959 and 0·0709, respectively, for the study watershed (Figure 2).

Model evaluation

Model efficiency criterion R^2 (Nash and Sutcliffe, 1970) was used to assess model performance. R^2 is defined as:

$$R^2 = 1 - \frac{\sum_{i=1}^{n}(Q_{mi} - Q_{si})^2}{\sum_{i=1}^{n}(Q_{mi} - \overline{Q_m})^2} \qquad (8)$$

where Q_{mi} is the measured discharge on the ith day, Q_{si} is the simulated discharge on the ith day, $\overline{Q}_m$ is the average measured discharge of the year, and n is the number of days in the year. The index has been widely used in various hydrological models and in many snowmelt runoff models (Hock, 1999; Pellicciotti *et al.*, 2005).

MODEL INPUT PARAMETERIZATION

Because the hydro-meteorological measurements for the study watershed are only available at the Yuzimen station, model inputs have to be either extrapolated from the station or derived from remotely sensed data. This section discusses how the inputs were parameterized for the model.

Temperature

Lapse rates are conventionally used to extrapolate measured air temperature at stations to different elevation zones. Most often, a global mean lapse rate of approximately 6·5 °C km^{-1} is used although lapse rates in mountain terrains show great diurnal and seasonal variations around the mean (Barry, 1992). Reliable local lapse rates and their temporal dynamics can be obtained if multiple weather stations at representative elevations in a watershed are available. For the study watershed, however, the only two available long-term weather stations (Hotan at 1375 m and Shiquanhe at 4280 m), which are 'close' to the watershed and with representative elevations, are about 200 and 500 km away from the watershed, respectively. Daily lapse rates for the period 2002–2004 were calculated with the measurements at the two stations. Locally smoothed mean daily lapse rates from the stations

show a distinct seasonal pattern (Figure 3). To verify the pattern, daily lapse rate was also calculated for the years at Hotan radiosonde station using the Integrated Global Radiosonde Archive (IGRA) dataset (Durre *et al.*, 2006). Locally smoothed mean daily lapse rates, which were derived from the radiosonde data using the temperatures measured at five pressure levels (i.e., 850, 700, 500, 400, and 300 mb), show a very similar temporal pattern to that obtained at the two stations. Daily lapse rates from the two sources are highly correlated with a correlation coefficient of 0.98. We therefore assumed that the daily lapse rates derived from the two weather stations, although outside the study watershed, could be used to extrapolate temperature in the study watershed.

The annual mean lapse rate derived from the two weather stations is $4.2\,°C\,km^{-1}$, which is much smaller than the global lapse rate of $6.5\,°C\,km^{-1}$. This implies less temperature decrease with elevation in the study watershed than the global average. In addition, daily lapse rate in the region shows a distinct seasonal pattern. At the end of January, the lapse rate starts increasing and reaches a plateau near the end of March. This plateau of high lapse rate lasts to the end of May. The lapse rate then starts decreasing and reaches its low valley during August. Then, it increases again and reaches a second peak in October. After that, the lapse rate declines quickly to the end of the year. It is interesting to see that a below-average lapse rate occurs during late summer months (middle July to middle September) which leads to higher temperature at high elevation for more snowmelt and matches the peak stream flows season observed in the watershed.

Precipitation

Extrapolating precipitation is particularly difficult in mountainous watersheds because of the lack of weather stations in the watershed and local factors, such as topography, which strongly influence the spatial distribution. Our first approach extrapolated precipitation at the Yuzimen station to the mean altitudes of the nine elevation zones by using an altitude gradient of 3.5% per 100 m as recommended by Martinec *et al.* (1998). In addition to extrapolation, we also explored the possibility of using the daily precipitation data from the Global Precipitation Climatology Project (GPCP), which is derived from multi-satellite observations with a spatial resolution of 1° by 1° (Huffman *et al.*, 2001). Because of the coarse spatial resolution, there are only four GPCP cells that cover the study watershed (Figure 4). The elevation zones were overlain with the GPCP cells and daily precipitation in each elevation zone was calculated based on the percentage of overlapping area each zone has with the intersecting GPCP cells.

Snow cover

Satellite-derived snow cover area is the best routinely available input for snowmelt runoff models especially in remote and data-scarce mountain watersheds (Compagnucci and Vargas, 1998; Lee *et al.*, 2005; Tekeli *et al.*, 2005). Compared with other satellite platforms, MODIS-derived snow cover area is most suitable for use in snowmelt model because of a higher spatial resolution (500 m) and location accuracy (Tekeli *et al.*, 2005). Although MODIS provides both daily and 8-day snow cover products, the 8-day maximum snow-cover extent (i.e. MOD10A2) product was used to minimize cloud cover.
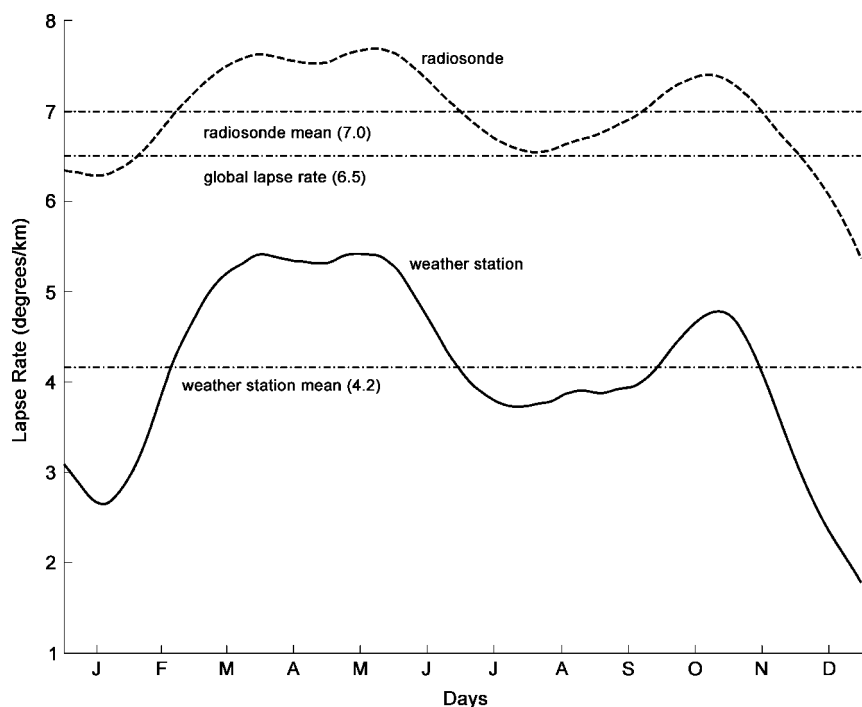

Figure 3. Daily lapse rates derived from radiosonde data (dotted curve) and calculated from two weather stations (solid curve)
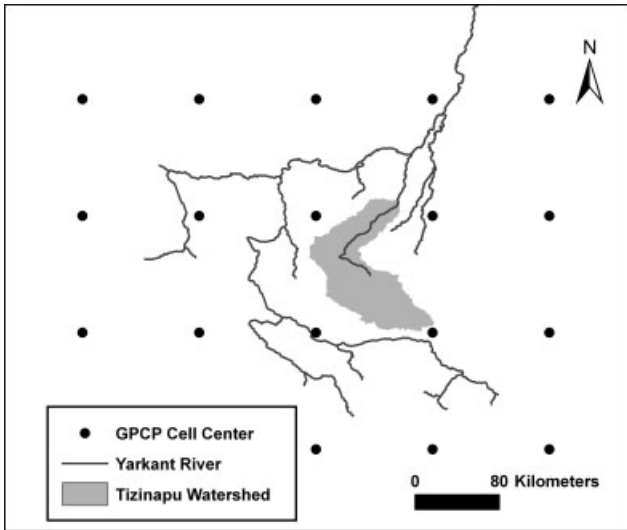
Figure 4. GPCP cell centres which cover the Tizinapu watershed

Even with the 8-day maximum snow cover extent product, clouds are still a problem (see the black dots in Figure 5). In addition, there is a large fluctuation of snow cover between February and April when neither the temperature nor stream discharge indicates snowmelt.

The fluctuation may be caused by thin transient snow or just a misclassification of snow in MOD10A2. To remove the clouds and the fluctuation, a backward temporal filter was developed. The filter calculates the frequency of snow occurrence within the past 32 days and assigns a cell as snow covered only if the snow frequency at the cell is greater than 75%. Snow cover percentages within the nine elevation zones were then calculated using the filtered 8-day snow cover data. Daily snow cover percentages in the elevation zones was then interpolated using piecewise cubic Hermite interpolation.

MODEL APPLICATION

All the model parameters were set as described above except for the m in Equation (1) and the c in Equation (2). The model was first run with all the possible input parameterizations as discussed in the previous section for year 2004. We first explored the effects of the two precipitation parameterizations. Numerous model runs were carried out using those two precipitation inputs with different m and c (with a range from 0·4 to 1 based on Martinec *et al.*, 1998) values and other input parameterizations. All of them showed a better
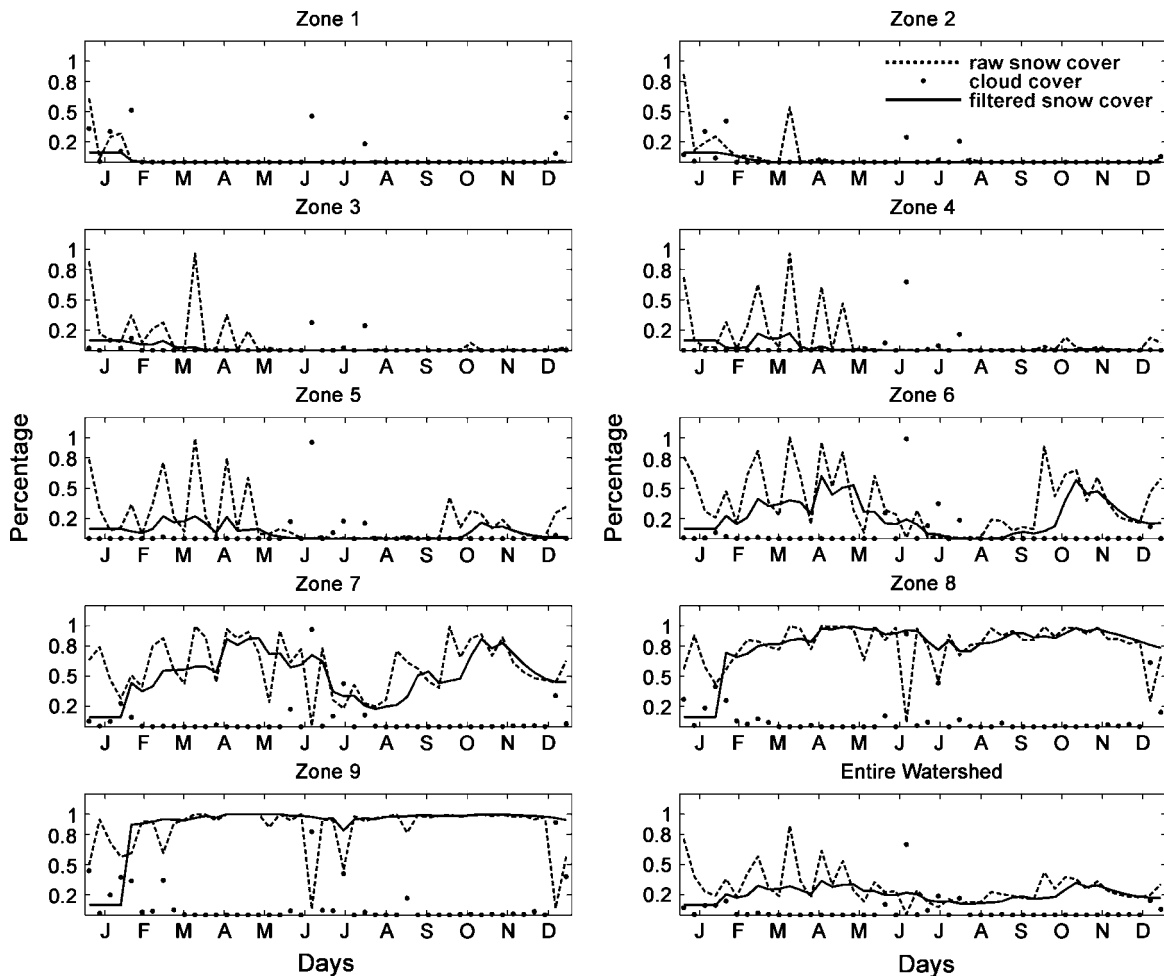

Figure 5. Raw (dotted line) and filtered (solid line) MODIS 8-day maximum snow cover percentages in the nine elevation zones and the entire watershed in 2004

performance without precipitation input. Precipitation at the Yuzimen station was further compared with the precipitation in the GPCP cell, which covers the station. The correlation coefficient between the two precipitation datasets is only 0·097. This indicates that neither the station nor the GPCP provides reliable precipitation data for the model. In addition, except for few spikes in late summer, the overall hydrograph resembles the discharge from a snow-/glacier-dominated watershed. All those factors made us decide to turn off the precipitation input for model calibration and validation.

The best model run for the year of 2004 with the precipitation input turned off has a R^2 value of 0·64 with a m value of 0·000 039 (m^2 cm W^{-1} h^{-1} $°C^{-1}$). This 'optimal' m value was obtained by systematically varying its value to run the model. This best model run was obtained using filtered MODIS snow cover, daily lapse rate calculated from the two weather stations, and the snow albedo directly scaled from MODIS snow cover. Measured and simulated daily discharges for the best model are shown in Figure 6.

For validation, the model was run for years 2003 and 2002. Measured and simulated daily discharges for those two years are shown in Figure 6. The R^2 values for years 2003 and 2002 are 0·78 and 0·51, respectively. Simulated hydrographs matched well with the snowmelt component of the measured hydrographs. The simulated hydrographs, especially in years 2003 and 2002, indicated that the lack of rainfall input was not heavily compensated during calibration. The model, however, did not simulate the peak stream flows well in August. The relative low R^2 values, obtained in our study

and their difference among the years, are attributed to the underestimates of those peak flows in the hydrographs. The low R^2 value in year 2002 might be caused by several extreme peak flows occurred in the year and the high R^2 value in 2003 could also be explained by mild stream flows in the year. We think that those peak stream flows might be caused by some extreme rainfall events in August. If this is true, then precipitation data is the major data limitation for improving model performance. Considering the size of the watershed and the limited measurements available, we think the model satisfactorily simulated daily stream flow for years 2002 to 2004.

Model sensitivity

To identify the primary input parameterizations to which the model are sensitive, the model was run with different parameterizations. Different ways of extrapolating temperature were first examined. The model was run with three additional lapse rates, i.e. the global lapse rate of 6·5 °C km^{-1}, the local mean lapse rate of 4·2 °C km^{-1}, and 3-year average daily lapse rate. Simulated and measured daily stream flows with those lapse rates are shown in Figure 7 and their corresponding R^2 values are listed in Table I.

As is shown in Table I and Figure 7, the model is very sensitive to lapse rate. The global lapse rate significantly underestimated daily stream flow. The local mean lapse rate performed much better than the global lapse rate. However, it still does not reflect the temporal variation of lapse rate in the region. Especially, the high lapse rate plateau in late spring (Figure 3) is missing when the local mean lapse rate is used. Because of this, the
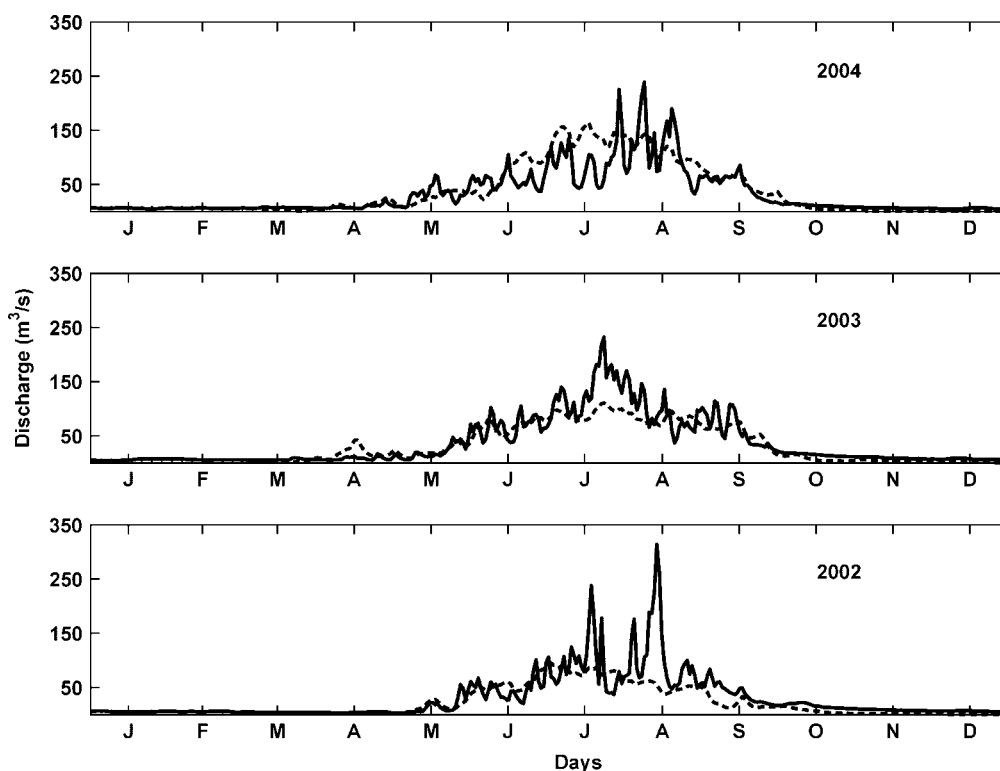

Figure 6. Simulated (dotted line) and measured daily discharge (solid line) for years 2004, 2003, and 2002
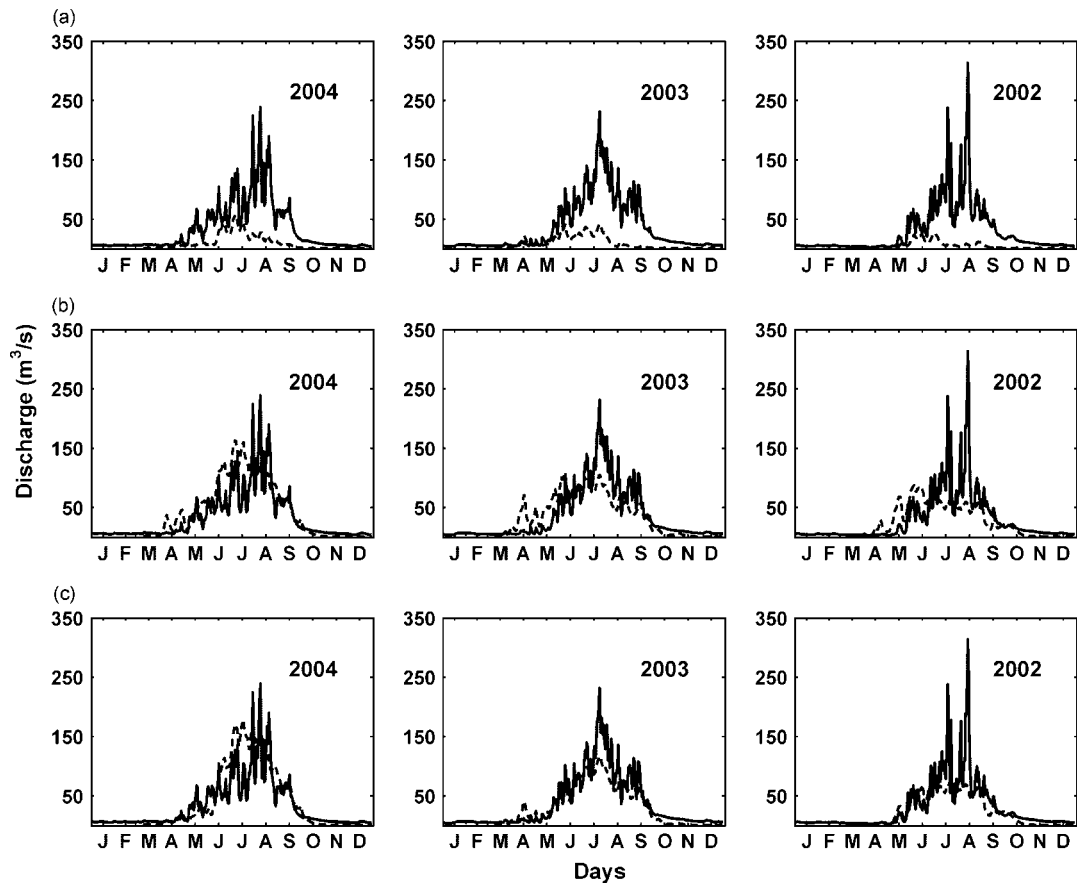
Figure 7. Simulated (dotted line) and measured (solid line) daily discharge using the global lapse rate of 6·5 °C km^{-1} (a), averaged local lapse rate of 4·2 °C km^{-1} (b), and averaged daily lapse rate from year 2002 to 2004 (c)

Table I. Model efficiency (R^2) with semi-distributed model inputs using different lapse rates

Year	2004	2003	2002
Global lapse rate of 6·5 °C	−0·03	−0·12	−0·24
Average local lapse rate of 4·2 °C	0·57	0·62	0·38
3-year average daily lapse rate	0·54	0·78	0·52
Individual year's daily lapse rate	0·64	0·78	0·51

Table II. Model efficiency (R^2) with lumped solar radiation and snow albedo inputs using different lapse rates

Year	2004	2003	2002
Global lapse rate of 6·5 °C	−0·11	−0·03	−0·27
Average local lapse rate of 4·2 °C	0·59	0·40	0·27
3-year average daily lapse rate	0·60	0·74	0·44
Individual year's daily lapse rate	0·67	0·78	0·42

model overestimated snowmelt in the spring season. The difference between 3-year average daily lapse rate and individual year's daily lapse rate is small although the latter performed much better in year 2004 (Table I). Those results indicated that the global lapse rate should not be used in this region and the temporal variation of lapse rate is very important for modelling the timing of snowmelt in the study watershed.

To investigate the effect of the snow cover filter, raw snow cover data was used to run the model with the parameters and all other inputs were set the same as the best model run. The R^2 values obtained for years 2004, 2003, and 2002 are 0·39, 0·56, and 0·36, respectively. Compared to the R^2 values (bottom row in Table I), which used filtered snow cover data, the frequency filter greatly improved model performance.

Semi-distributed versus lumped inputs

All the model runs discussed above are semi-distributed because they used the nine elevation zones as model spatial units. To see how lumped inputs may affect the model results, solar radiation and snow albedo inputs were lumped over the entire watershed and then used in model runs. The best R^2 value achieved for year 2004 was 0·67 with an 'optimal' m value of 0·000035 (m^2 cm W^{-1} h^{-1} °C^{-1}). Using this m value, R^2 values from the model runs for years 2003 and 2002 were 0·78 and 0·42, respectively. Compared to the results from semi-distributed inputs (the bottom row in Table I), lumped model inputs gave a little better performance in 2004, the same in 2003, and somewhat worse in 2002.

Sensitivity of the lumped model inputs to different lapse rates was also examined. The results are summarized in Table II. Like the semi-distributed model, the lumped model is very sensitive to lapse rate. The model
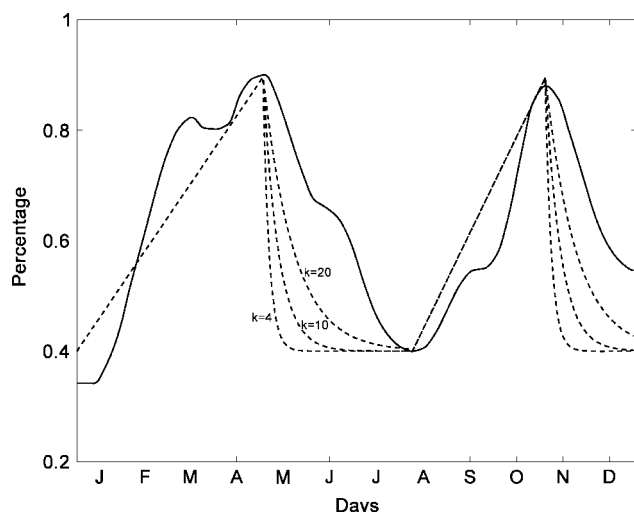
Figure 8. Daily snow albedo in year 2004 for the entire watershed as derived from snow cover percentage (solid line) and calculated by using Equation (3) with k set to 4, 10, and 20 (dotted lines)

Table III. Model efficiency (R^2) with semi-distributed model inputs using different snow albedo parameterizations

Year	2004	2003	2002
$K = 4$	0·17	0·49	0·27
$K = 10$	0·22	0·58	0·31
$K = 20$	0·35	0·71	0·37
Scaled from snow cover percentage	0·64	0·78	0·51

performed better when the lapse rate reflects local and temporal characteristics of the watershed.

Sensitivity of the model to snow albedo parameterizations was also examined. The two albedo parameterizations were compared. The first albedo parameterization was tested using three different k values ($k = 4$, 10, and 20 in Equation (3)), as suggested by Kondo and Yamazaki (1990). The second parameterization scales daily snow cover percentage directly into snow albedo using Equation (4). Daily snow albedo in year 2004 from the two parameterizations is shown in Figure 8. It can be noted in Figure 8 that S_{min} in Equation (4) is found during the summer days. The R^2 values for the two parameterizations are shown in Table III. The model is very sensitive to snow albedo parameterization. Smaller k values, which were suggested by Kondo and Yamazaki (1990) and USACE (1956), performed much worse than larger k values. As the k value increases, model performance improves and the snow albedo curve looks more like snow cover percentage curve. This observation led us to the second albedo parameterization which directly scales snow cover percentage into snow albedo.

CONCLUDING REMARKS

The study has shown that a temperature-index snowmelt runoff model, in which DDF is varied by solar radiation and snow albedo, can be used to satisfactorily simulate daily stream flow in an arid mountain watershed

where only limited hydro-meteorological measurements are available. Sensitivity analysis indicated that the model was strongly influenced by the lapse rate used to extrapolate temperature and the snow albedo which regulates the amount of available solar radiation for snowmelt. The distinct seasonal pattern of lapse rate played a key role for successful simulation. The high correlation between lapse rates derived from two weather stations and calculated from radiosonde data implied that radiosonde data might be used to estimate surface lapse rate when weather station data are not available.

The snow-albedo parameterization which directly scales snow cover percentage into snow albedo worked well for the watershed although further validation is needed. In addition, the snow cover filter, which filtered out clouds and large fluctuation of snow cover from the raw MODIS snow cover data, improved model performance. Semi-distributed model, where all the inputs are unique in the nine elevation zones, did not significantly improve model performance. Like the semi-distributed model, lumped models are also very sensitive to lapse rates.

The model, however, did not simulate the peak stream flows well as most of the good model runs underestimated the peak discharges occurred in August. There is still no good explanation for the tremendous variation of stream flow in August, especially in years 2004 and 2002. The variation could be caused by heavy precipitation events. Unfortunately, this cannot be validated with the current precipitation measurement at the Yuzimen station or the precipitation data from GPCP.

Several forms of combining temperature-dependent and temperature-independent components in a semi-temperature-index model were compared by Pellicciotti *et al*. (2005). Future research on improving our model will explore those options. The spatial units of our current model were based on elevation zones. This tessellation has no allowance for representing the variations of slope, aspect, land cover, and melt within zones. Between the elevation zone and grid cell approaches, there stands the possibility of generating snow response units delineated not just by elevation but also slope, aspect, and other topographic controls. This approach corresponds to the concept of hydrological response units in rainfall–runoff modelling. In the future, we will explore the idea of snowmelt-response units which are the largest areas within which subscale spatial variability does not significantly affect basin response, and can be averaged or represented statistically. The large fluctuation of snow cover in zones 4, 5 and 6 in the spring (Figure 5) also calls for further validation on MODIS snow cover products.

REFERENCES

Arendt A, Sharp M. 1999. Energy balance measurements on a Canadian high arctic glacier and their implications for mass balance modelling. In *Interactions Between the Cryosphere, Climate and Greenhouse Gases, Proceedings of the IUGG Symposium*, Tranter M, Armstrong R, Brun E, Jones G, Sharp M, and Williams M (eds). IAHS Publication No. 256. IAHS Press: Birmingham; 165–172.

Barry RG. 1992. *Mountain Weather and Climate*, 2nd edn. Routledge: London; 402.

Bloschl G. 1991. The influence of uncertainty in air temperature and albedo on snowmelt. *Nordic Hydrology* **22**: 43–69.

Braun LN, Grabs W, Rana B. 1993. Application of a conceptual precipitation-runoff model in the Langtang Khola basin, Nepal Himalaya. In *Snow and Glacier Hydrology, Proceedings of the Kathmandu Symposium*, Young GJ (ed.). IAHS Publication No. 218. IAHS Press: Wallingford, Oxfordshire; 221–237.

Brock BW, Willis IC, Sharp MJ. 2000. Measurement and parameterization of albedo variations at Haut Glacier d'Arolla, Switzerland. *Journal of Glaciology* **46**: 675–688.

Cazorzi F, Dalla Fontana G. 1996. Snowmelt modelling by combining air temperature and a distributed radiation index. *Journal of Hydrology* **181**: 169–187.

Compagnucci RH, Vargas WM. 1998. Inter-annual variability of the Cuyo rivers' streamflow in the Argentinean and Andeas Mountains and ENSO events. *International Journal of Climatology* **18**: 1593–1609.

Daly SF, Davis R, Ochs E, Pangburn T. 2000. An approach to spatially distributed snow modelling of the Sacramento and San Joaquin basins, California. *Hydrological Processes* **14**: 3257–3271.

Dozier J, Frew J. 1990. Rapid calculation of terrain parameters for radiation modeling from digital elevation data. *IEEE Transactions on Geoscience and Remote Sensing* **28**: 963–969.

Dunn SM, Colohan RJE. 1999. Developing the snow component of a distributed hydrological model: a step-wise approach based on multi-objective analysis. *Journal of Hydrology* **223**: 1–16.

Durre I, Vose RS, Wuertz DB. 2006. Overview of the integrated global radiosonde archive. *Journal of Climate* **19**: 53–68.

Ferguson RI. 1999. Snowmelt runoff models. *Progress in Physical Geography* **23**: 205–227.

Findlay AM. 1998. Policy implications of population growth in arid environments. In *Population and Environment in Arid Regions*, Clarke JI, Noin D (eds). Parthenon Publishing Group: Pear River; 384.

Fu P, Rich PM. 1999. Design and implementation of the Solar Analyst: an ArcView extension for modeling solar radiation at landscape scales. In *Proceedings of ESRI Annual User Conference*, Redlands, (http://gis.esri.com/library/userconf/proc99/proceed/papers/pap867/p867.htm, last accessed on May 19, 2008).

Hall DK, Riggs GA, Salomonson VV, DiGirolamo NE, Bayr KJ. 2002. MODIS snow-cover products. *Remote Sensing of Environment* **83**: 181–194.

Hock R. 1999. A distributed temperature-index ice- and snowmelt model including potential direct solar radiation. *Journal of Glaciology* **45**: 101–111.

Huffman GJ, Adler RF, Morrissey MM, Bolvin DT, Curtis S, Joyce R, McGavock B, Susskind J. 2001. Global precipitation at one-degree daily resolution from multisatellite observations. *Journal of Hydrometeorology* **2**: 36–50.

IPCC. 2007. Climate Change 2007-the physical science basis. In *Contribution of Working Group I to the Fourth Assessment Report of the Intergovernmental Panel on Climate Change*, Solomon S, Qin D, Manning M, Chen Z, Marquis M, Averyt KB, Tignor M, Miller HL (eds). Cambridge University Press: Cambridge, New York; 996.

Kane DL, Gieck RE. 1997. Snowmelt modeling at small Alaskan arctic watershed. *Journal of Hydrologic Engineering* **2**: 204–210.

Kondo J, Yamazaki T. 1990. A prediction model for snowmelt, snow surface temperature and freezing depth using a heat balance method. *Journal of Applied Meteorology* **29**: 375–384.

Lee S, Klein AG, Over TM. 2005. A comparison of MODIS and NOHRSC snow-cover products for simulating streamflow using the snowmelt runoff model. *Hydrological Processes* **19**: 2951–2972.

Martinec J. 1975. Snowmelt-runoff model for stream flow forecasting. *Nordic Hydrology* **6**: 145–154.

Martinec J, Rango A. 1986. Parameter values for snowmelt runoff modeling. *Journal of Hydrology* **84**: 197–219.

Martinec J, Rango A, Robert R. 1998. *Snowmelt Runoff Model (SRM) User's Manual*, (http://hydrolab.arsusda.gov/cgi-bin/srmhome last accessed on May 19, 2008).

Nash JE, Sutcliffe JV. 1970. River flow forecasting through conceptual models. Part 1. A discussion of principles. *Journal of Hydrology* **10**: 282–290.

Pellicciotti F, Brock B, Strasser U, Burlando P, Funk M, Corripio J. 2005. An enhanced temperature-index glacier melt model including the shortwave radiation balance: development and testing for Haut Glacier d'Arolla, Switzerland. *Journal of Glaciology* **51**: 573–587.

Pipes A, Quick MC. 1987. Modelling large scale effects of snow cover. *International Association of Hydrological Sciences Publication* **166**: 151–160.

Schreider SY, Whetton PH, Jakeman AJ, Pittock AB. 1997. Runoff modelling for snow-affected catchments in the Australian alpine region, eastern Victoria. *Journal of Hydrology* **200**: 1–23.

Tekeli AE, Akyurek Z, Sorman AA, Sensoy A, Sorman AU. 2005. Using MODIS snow cover maps in modeling snowmelt runoff process in the eastern part of Turkey. *Remote Sensing of Environment* **97**: 216–230.

Thornton PE, Hasenauer H, White MA. 2000. Simultaneous estimation of daily solar radiation and humidity from observed temperature and precipitation: an application over complex terrain in Austria. *Agricultural and Forest Meteorology* **104**: 255–271.

U.S. Army Corps of Engineers. 1956. *Snow Hydrology: Summary Report of the Snow Investigation*. North Pacific Division: Portland; 462.

U.S. Army Corps of Engineers. 1998. *Runoff from Snowmelt*. University Press of the Pacific: Honolulu, HI; F–14.